ACS APPLIED MATERIALS & INTERFACES

Caltech Library

Subscriber access provided by Caltech Library

Energy, Environmental, and Catalysis Applications

Micropore-Boosted Layered Double Hydroxide Catalysts#EIS Analysis in Structure and Activity for Effective Oxygen Evolution Reaction

Cui Ye, Min Qiang Wang, Shu-Juan Bao, and Changhui Ye

ACS Appl. Mater. Interfaces, **Just Accepted Manuscript** • DOI: 10.1021/acsami.9b09144 • Publication Date (Web): 01 Aug 2019

Micropore-Boosted Layered Double Hydroxide Catalysts：EIS Analysis in Structure and Activity for Effective Oxygen Evolution Reaction

Cui Ye,[*,†] *Min-Qiang Wang,*[‡,§] *Shu-Juan Bao,* [‡] *Changhui Ye*[*,†]

[†]College of Materials Science and Engineering, Zhejiang University of Technology, Hangzhou 310014, China

[‡]Institute for Clean Energy & Advanced Materials, Faculty of Materials and Energy, Southwest University, Chongqing 400715, China

[§]Division of Engineering and Applied Science, California Institute of Technology, Pasadena, CA 91125, USA

ABSTRACT Since the oxygen evolution catalysis process is vital yet arduous in the energy conversion and storage devices, it is highly desirous but extremely challenging to engineer earth-abundant, noble-metal-free nanomaterials with superior electrocatalytic activity toward effective oxygen evolution reaction (OER). Herein, we construct a prism-like cobalt-iron layered double hydroxide (Co-Fe LDH) with a Co/Fe ratio of 3:1 utilizing a facile self-templated strategy. Instead of carbon species-coupled treatment, we focus on ameliorating the intrinsic properties of LDHs as an OER electrocatalyst accompanied with hierarchical nanoflake shell, well-defined interior cavity and numerous microporous defects. In contrary to conventional LDHs synthesized *via* a one-pot method, Co-Fe LDHs fabricated in this work possess a huge specific surface area up to 294.1 m^2 g^{-1} that not only provide abundant active sites, but also expedite the kinetics of

OER process. The as-prepared Co-Fe LDH electrocatalysts exhibit advanced electrocatalytic performance, and a dramatic stability of OER in an alkaline environment. Particularly, the contribution of micropore defects is clearly discussed according to the EIS analysis, in which the time constant of OER at the micropore defect is several orders of magnitude smaller than that at the exterior of Co-Fe LDHs, forcefully verifying the intrinsic catalytic activity enhancement derived from the micropore defects. This work provides a promising model to improve OER electrocatalysts activity *via* produce defects and research the contribution of micropore defects.

KEYWORDS: LDH electrocatalysts, micropore defects, EIS analysis, oxygen evolution reaction, wettability

INTRODUCTION

As the rapid consumption of fuel resources led to an increasingly serious environmental problem, efficient electrolytic water splitting has been considered as an promising strategy to meet the urgent demands of converting and storing energies.[1-4] Unfortunately, the anodic oxygen evolution reaction (OER) of water splitting involves a four-proton-coupled electron transfer process with high overpotential and sluggish kinetics, which hinders overall water splitting efficiency.[5,6] Generally, superior electrocatalysts with a low overpotential in OER process are those state-of-the-art noble-metal-based catalysts, such as IrO_2 and RuO_2, which are costly with finite resource.[7,8] Nevertheless, recent studies reported that it is feasible to use noble-metal-free materials as electrocatalysts for efficient OER.[9-11] And among these promising alternatives, transition metal layered double hydroxides (LDHs) have attracted much attention due to their tunable chemical composition, environment-friendly peculiarity, and cost effectiveness.[12-14] They

have a universal formula of $[M^{2+}_{1-x}M^{3+}_{x}(OH)_2]^{x+}\cdot[A^{n-}_{x/n}]^{x-}\cdot mH_2O$, and consist of positively-charged host layers and weakly bound charge-balancing interlayer hydrated anions. In particular, LDHs possess high ionic conductivity and superior stability in alkaline environment, which makes it potential to be applied as efficient electrocatalyst for OER.[15,16]

LDHs bid fair to be high-performance electrocatalysts with the first row transition-metal elements containing Co, Fe or Ni in the host layer composition.[17-19] More recently, to pursue enhanced catalytic activity, efforts have been devoted into the synergistic effects and charge-transfer kinetics of carbon species-coupled LDHs. However, little attention has been paid to the intrinsic properties of LDHs.[20-22] It is well-known that the oxidation reaction facilitates the production of a catalytical active phase with the high valence, but in some aspects the process can be hindered by the close-packed basal planes.[3,23-25] The key to promoting the intrinsic catalytic activity of LDHs is to rationally adjust surface properties or increase the number of active sites.[19] A facile self-templated strategy has the potential to engineer LDH nanostructures for achieving advanced electrocatalytic performance,[26-28] in comparison with the one-pot strategies, such as electrodeposition, hydrothermal reaction, and others.[29,30]

Nowadays, the self-templated strategy, directly and efficiently converting templates into hollow structures especially with complex architectures, has attracted increasing attention. [31-33] Lou's group pioneered in advanced self-templated methods and elegantly divided them into three categories, including "Selective etching", "Outward diffusion" and "Heterogeneous contraction".[27] To establish well-defined multiple or hierarchical hollow structure, "Outward diffusion" is applied by relocating the mass in templates from inner region to outer region.[27,28] Based on the self-templated strategy, structural defects are expected to arise in LDHs fabrication process. It is worth mentioning that the structural defects are beneficial to boost the activity of

electrocatalyst *via* the vast active sites exposure and superior charge transport capabilities, certified by more and more studies.[19] Although more and more studies have certified the significant effect of defects on electrocatalyst, the contribution and cause of structural defects to the overall electrocatalytic performance of catalyst is rarely studied. Generally, electrochemical impedance spectroscopy (EIS) is an effective technique, in which the impedance of an electrochemical system is studied as a function of the frequency of an applied a.c. wave. When a steady-state system is perturbed (say by an applied a.c. voltage), it relaxes to a new steady state. The time (in seconds) taken for this relaxation is known as the time constant "τ", and the analysis of relaxation process would provide information about the system. In the case of the frequency domain, the fast processes with a low time constant occur at high frequencies, while the slow processes with a high time constant occur at low frequencies.[34,35]

Herein, we constructed a highly efficient and LDHs-based OER catalyst through the self-templated strategy. The defective Co-Fe LDHs exhibit remarkable OER activity and excellent stability primarily by integrating the advantages of defect-boosted structure and superior charge transport capability. More importantly, we clearly observe the defects structure and deeply discusses the contribution of micropore defects. On account of EIS data, the time constant of OER at the micropore defects is several orders of magnitude smaller than that at the exterior of Co-Fe LDHs, forcefully certifying the good electrocatalytic activity derived from the micropore defect. In addition, the good wettability of the defective Co-Fe LDHs further contribute to high electrocatalytic performance. The findings in this work are conducive to the development of a viable route to designing cost-effective electrocatalysts for OER.

EXPERIMENTAL SECTION

Synthesis of the Co precursor

The Co precursor was synthesized according to the literature work with a little modification.[28] $C_4H_{14}CoO_8$ (0.35 g) and PVP (0.75 g) were dissolved and ultrasonically mixed for 5 min in ethanol (50 mL) at room temperature. The obtained mixture was transferred into a 250 mL round-bottom flask, and then heated and refluxed at 90 °C under vigorous magnetic stirring for 5 h. Afterwards, the product was washed by centrifuging (5 min, 10000 rpm) with ethanol and ultrapure water for several times, and dried under vacuum to collect the Co precursor.

Synthesis of the Co-Fe layered double hydroxide (LDH)

The Co precursor (20 mg) was ultrasonically dispersed in ethanol (2 mL) as solution A. $FeSO_4 \cdot 7H_2O$ (10 mg) was ultrasonically dissolved in ultrapure water (5 mL) followed by the addition of ethanol (5 mL), and this solution was denoted as solution B. Next, solution A and solution B were mixed quickly, and aged for 10 min under N_2 protection. A green precipitate of Co-Fe LDHs was collected, followed by centrifuging and washing with ethanol for several times, and drying in vacuum oven.

Electrochemical Performance

All electrochemical measurements were executed on a workstation (CHI 660E, CHI Instruments Inc, Shanghai) in a three-electrode setup, coupled with a graphite electrode as a counter electrode, Hg/HgO (1 M NaOH) electrode as a reference electrode, and a modified rotating disk electrode (RDE, Φ = 4 mm) as a working electrode. To prepare the working electrode, the catalyst powder (2 mg) was added in a solution (1 mL) of ethanol-ultrapure water (1:1 by vol) and Nafion (1 wt.%), and ultrasonically dispersed to obtain homogeneous catalyst ink. Then, the ink (2 mg mL^{-1}, 10 μL) was dropped onto the well-polished RDE surface, and air-dried at

ambient environment. KOH solution (1 M) was utilized as the electrolyte during the whole test, and the rotation rate of the RDE is 1600 rpm. The polarization curves were surveyed by the linear sweep voltammetry (LSV) in the range of 0.2 ~ 0.8 V *vs.* Hg/HgO at a scan rate of 5 mV s^{-1} with 95% *iR* correction. Particularly, 20 cycles of cyclic voltammetry (CV) measurements at a scan rate of 50 mV s^{-1} were executed to stabilize the current before the LSV test. To dynamically evaluate the OER kinetics of catalysts, polarization curves were plotted by the potential versus logarithm current density (*j*). The stability was studied using LSV and amperometric *i*−*t* methods at a fixed potential. Electrochemical impedance spectroscopy (EIS) was measured by applying an AC amplitude of 5 mV over the frequency range of 10^6 ~ 10^{-1} Hz. In this study, the recorded potential was all quoted against the reversible hydrogen electrode (RHE) by the equation: $E_{RHE} = E_{Hg/HgO} + 0.098 + 0.059$ pH. The overpotential (η) was calculated based on the following formula: $\eta = E_{RHE} - 1.23$ V. The current density was calibrated *via* dividing the current by geometric area of the working electrode.

RESULTS AND DISCUSSION

Figure 1a depicts the fabrication process of defect-boosted Co-Fe LDHs based on a self-templated strategy using a Co precursor. The crystal structures of the as-prepared samples were inquired by X-ray diffraction (XRD). As illustrated in Figure S1, the XRD pattern of the Co precursor reveals the diffraction peaks that could be assigned to cobalt acetate hydroxide (JCPDS No. 22-0582). When a suitable content of Fe ions was incorporated, all the broadened diffraction peaks in Figure 1b could be indexed to Co-Fe LDHs (JCPDS No. 50-0235). The results demonstrated LDH structures are produced effectively. In the rest of the paper, unless otherwise stated, we mention Co-Fe LDHs as that with a Co/Fe ratio of 3:1 for convenience, which refers

to the initial ratio in the synthetic process. From field-emission scanning electron microscopy (FESEM) images (Figure 1c, d), it can be seen that the individual Co precursor exhibits a smooth prismatic architecture and the prisms have a length of approximately 500 nm. Transmission electron microscopy (TEM) images of the Co precursor further illustrate the compact and solid characteristics of the samples (Figure S2). For Co-Fe LDHs, FESEM image confirms the retention of the prismatic architecture (Figure 1e), however, the smooth surface eventually becomes hierarchical shells composed of disorderly oriented nanoflakes. For comparison, the FESEM images with various Co/Fe ratios are shown in Figure S3. The results illustrate the obvious influence of Fe incorporation towards the morphology of samples with various Co/Fe ratios, in which the prismatic architectures are gradually collapse into disordered nanoflakes with the increasing amount of Fe ions. Figure 1f displays the results of energy-dispersive X-ray spectroscopy (EDX) mapping, which clearly confirms the presence and the uniform distribution of Co and Fe in LDH structures. LDH prisms with hierarchical shells and well-defined inner cavity are further exhibited in TEM images (Figure 1g, h), where abundant porous structure with loosely interconnected Co-Fe LDH nanoflakes can be observed. Figure 1i, S4 show high-resolution TEM (HRTEM) images of Co-Fe LDHs, from which a set of dislocations, lattice distortions, and micropore defects are observed. This unique structural feature provides rich active sites and a brilliant mass transfer pathway. Besides, the TEM images with various Co/Fe ratios are shown in Figure S5. Integrating the FESEM and TEM images towards the Co/Fe ratios of 6:1, 3:1, 3:2, and 1:1, prismatic architectures are gradually collapse into disordered nanoflakes with the increasing amount of Fe ions, while we can only observe the abundant porous structure with loosely interconnected nanoflakes in the Co/Fe ratio of 3:1. The results illustrate the obvious influence of Fe ions incorporation towards the morphology of Co/Fe ratios, and only the

3:1 ratio resulted in the complete formation of Co-Fe LDH structures, which is consistent with the generally acknowledged phenomena that x in the universal formula of LDHs should lie in the range 0.2-0.33 to stabilize LDH compounds.[39] Figure 1j exhibits lattice fringes with a *d*-spacing of 0.26 nm that can be indexed to (012) lattice planes of Co-Fe LDHs. The inset in Figure 1j shows the corresponding Fast Fourier Transform (FFT) pattern, corresponding well to XRD results in Figure 1b.

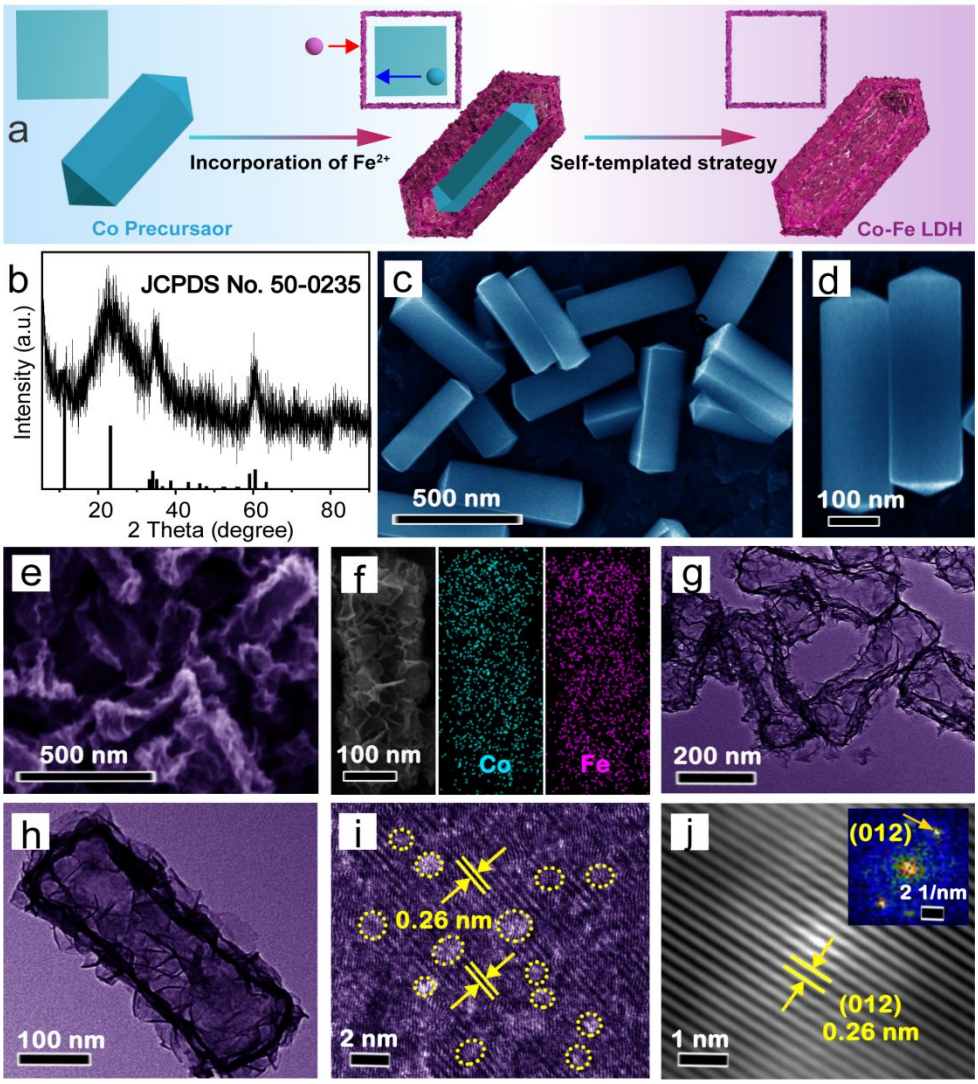

Figure 1. a) The fabrication process of defect-boosted Co-Fe LDHs. b) XRD pattern of Co-Fe LDHs. FESEM images of c, d) Co precursor, and e) Co-Fe LDHs. f) Elemental mapping of an individual Co-Fe LDH prism. g) TEM image, h, i) HRTEM image, and j) simulated HRTEM image and FFT pattern (inset) of Co-Fe LDHs.

Typical X-ray photoelectron spectroscopy (XPS) was employed to investigate the chemical composition and surface electronic states of Co-Fe LDHs. As shown in Figure S6a, the overview survey spectrum indicates the coexistence of Co, Fe, O, and C elements in samples with different binding energies (BE). The spectral peaks at 531.8 and 284.5 eV belong to O1s and C1s, respectively (Figure S6b, c). The high-resolution XPS of Co 2p spectrum (Figure 2a) is split into Co $2p_{3/2}$ and Co $2p_{1/2}$, located at 781.4 and 797.5 eV, respectively, accompanied by two satellite peaks. The prominent Co $2p_{3/2}$ satellite peak is generally considered an indicator of a high-spin Co^{2+} state. [14,20] The Fe 2p spectrum has been fitted into two BE peaks at 711.6 and 725.4 eV due to Fe $2p_{3/2}$ and Fe $2p_{1/2}$, respectively (Figure 2b). Considering the BE difference of 13.8 eV, it is believed that the Fe species exist in the form of Fe^{3+}.[23] Figure 2c displays the Raman spectrum of Co-Fe LDHs. Characteristic peaks at 456 and 535 cm^{-1} are observed, and attributed to the vibration modes of Metal-Oxygen-Metal (M-O-M) bond.[36] These results unambiguously confirm the successful formation of Co-Fe LDHs.

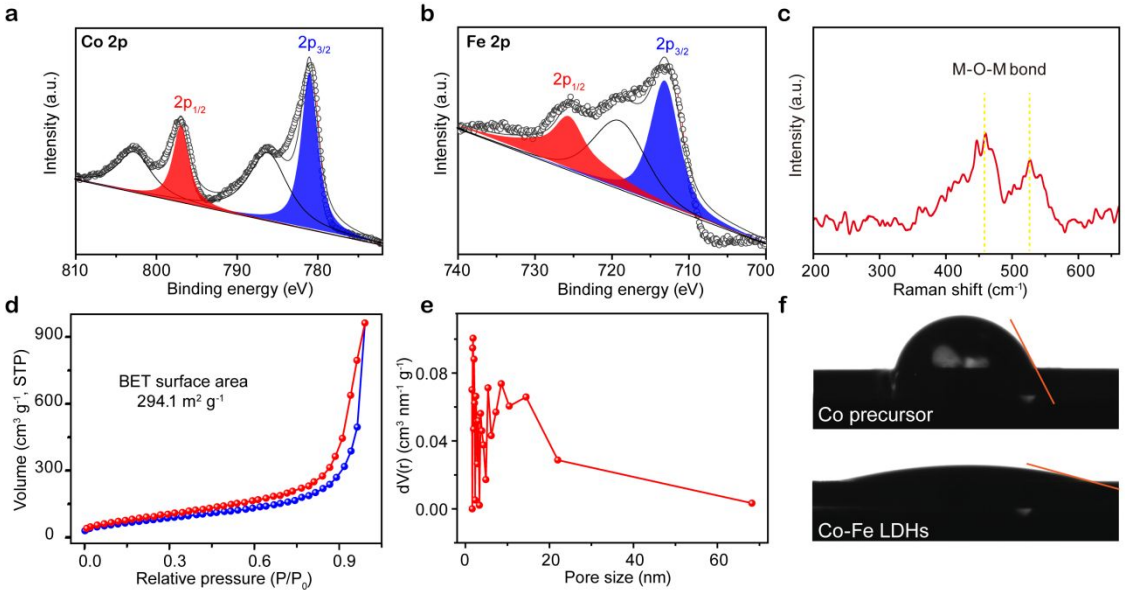

Figure 2. XPS analysis of a) Co 2p region, and b) Fe 2p region for Co-Fe LDHs. c) Raman spectrum of Co-Fe LDHs. d) Nitrogen adsorption–desorption isotherm, and e) the corresponding pore size distribution of Co-Fe LDHs. f) Contact angle measurements.

As a key factor for electrocatalyst, Brunauer-Emmett-Teller (BET) specific surface area and porosity distribution were evaluated by N_2 adsorption/desorption isotherms (Figure 2d, e) using Barrett–Joyner–Halenda (BJH) method. Co-Fe LDHs with hierarchical prismatic structure have a high BET surface area of 294.1 m^2 g^{-1} which is greater than that of recently reported LDH electrocatalysts.[17,19] The average pore diameter is calculated as 1.4 nm. The hysteresis of the curve initiating from a low P/P_0 value implies the microporous structure of the loosely packed LDH nanoflakes, which is consistent with TEM observations in Figure 1i. As we discussed in the previous section, the incorporation of Fe ions in Co precursor generated numerous micropore defects in crystal lattices of Co-Fe LDHs. Undoubtedly, engineering affluent defects into Co-Fe LDHs facilitates exposure of abundant active sites, thereby enhancing electrocatalytic activity. Figure 2f depicts the static contact angles of Co precursor and Co-Fe LDHs. Co-Fe LDHs have a much smaller contact angle than that of the Co precursor, revealing a more hydrophilic surface of the former. The good surface wettability of the catalyst facilitates electrolyte penetration and accelerates hydroxyl group migration and oxygen release.[36] Therefore, this result portends the good OER performance derived from the defect-rich structures based on the self-templated strategy.

We thoroughly explored and analyzed the key factors related to electrocatalytic activity and gained insight into OER performance. The effect of Co/Fe ratio in LDH prisms on polarization curves was investigated. As depicted in Table S1 and Figure 3a, LDH prisms with a Co/Fe ratio of 3:1 possess the lowest onset potential and the highest current density at 1.65 V (*vs.* RHE). To analyze the electrochemical active surface area (ECSA), the double-layer capacitance (C_{dl}) was characterized by CV at a suitable potential range without a redox process (Figure S7). Figure 3b shows the C_{dl} of samples at the Co/Fe ratios of 6:1, 3:1, 3:2, and 1:1, respectively. The sample

with a Co/Fe ratio of 3:1 displayed the largest C_{dl} in accordance with the analysis result of polarization curves, certifying that the incorporation of Fe ions in an appropriate ratio contributed to the improvement of OER activity. In addition, the turnover frequencies (TOFs), directly related to actual number of active sites, are calculated to reveal the inherent properties of Co-Fe LDHs for OER. As shown in Figure 3c, as-prepared Co-Fe LDHs with a Co/Fe ratio of 3:1 have a TOF of 0.312 s^{-1}, which is the largest among Co-Fe LDH samples in this work.

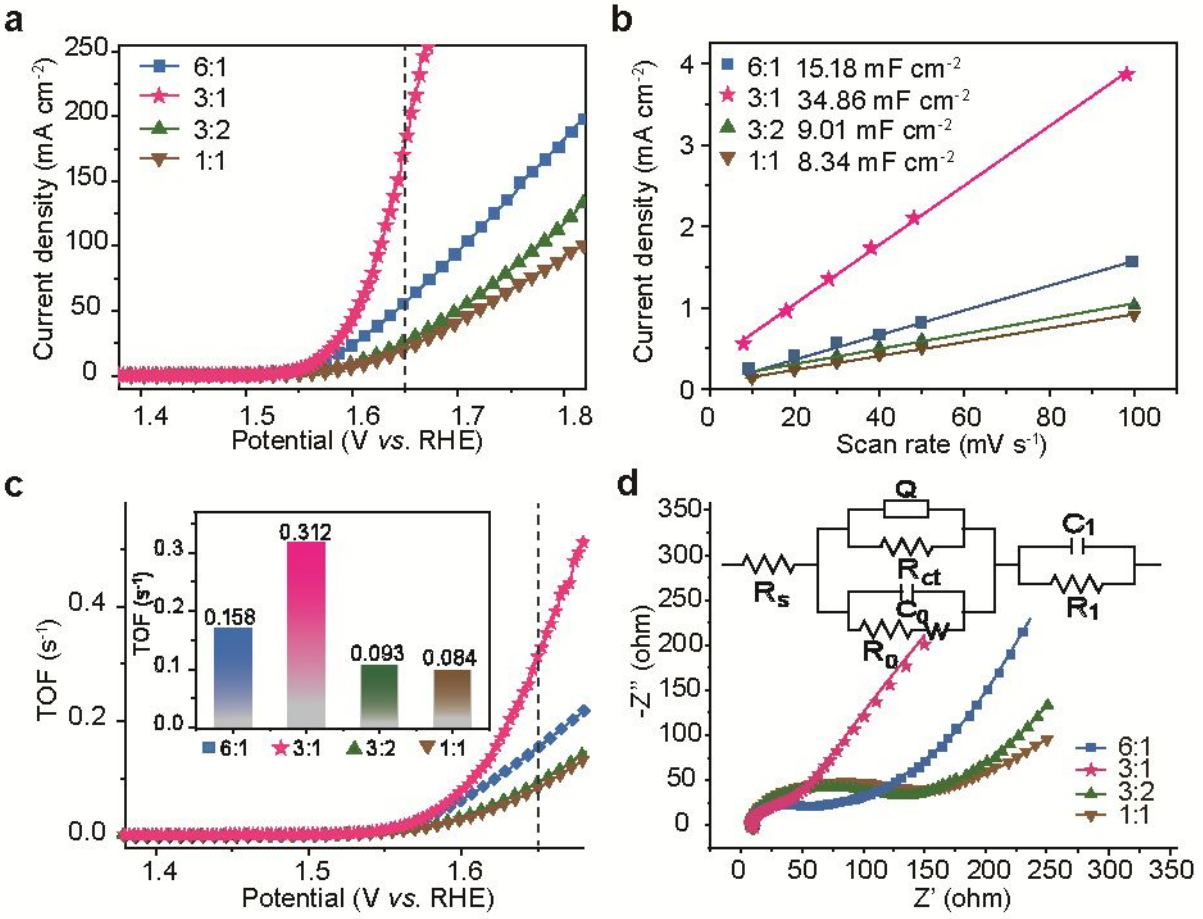

Figure 3. a) Polarization curves, b) Current density differences plotted against scan rates under a non-Faradaic range. c) TOFs of Co-Fe LDHs at different Co/Fe ratios of 6:1, 3:1, 3:2 and 1:1 (inset shows the TOF values at 1.65 V *vs.* RHE for different Co/Fe ratios of Co-Fe LDHs). d) Nyquist plots with a fitted equivalent circuit (inset).

Both the electrochemical measurements provide electrocatalytic properties averaged over all active sites on the surface of LDHs, thereby obscuring the true contribution of elementary processes. In order to understand in depth the contribution of micropore defects to the overall electrocatalytic performance, we performed electrochemical impedance spectroscopy (EIS) measurements on Co-Fe LDH samples, taking into account that EIS was a powerful tool for decoupling the electrochemical processes in complex electrodes. Figure 3d presents the Nyquist plots and fitting results for EIS measurements with a proper equivalent circuit model for Co-Fe LDHs with different Co/Fe ratios. In the equivalent circuit model, R_s corresponds to the series resistance of the electrolyte, the electrodes, and the circuit leads. The two *RC* circuits in the middle of the diagram describe the charge kinetics at the interface between the electrolyte and the outer surface as well as the micropore defects of Co-Fe LDHs, respectively. The third *RC* circuit is associated with adsorption/desorption of the intermediates of the OER. Obviously, the Nyquist plot of LDHs with a Co/Fe ratio of 3:1 possesses the smallest semicircle diameter in the high frequency region, indicating that proper incorporation of Fe ions in LDH prisms enabled ultrafast charge transfer at the electrolyte/electrode interface. The minimum R_s value also indicates that LDHs with a Co/Fe ratio of 3:1 has the highest conductivity among the four compositions. In Table S2, we can unambiguously assign the high frequency semicircle in EIS curves to the kinetic process at the interface between the electrolyte and the micropores in the working electrode. The much smaller time constant provides conclusive evidence that the active sites on the surface of the micropore defects are much more effective in electrocatalytic OER, in good agreement with previous observations by other researchers.[3,9,34] It was proposed that the synergistic effect of Co and Fe in LDHs lowered the energy barrier of OER, thereby accelerating the reaction kinetics.[37-39] We found that the synergistic effect is more effective for the active sites

at the surface of the micropore defects. The capacitance of the micropore defects is much larger than that of the outer surface of the electrodes, further confirming the higher electrocatalytic activity of the micropore defects in Co-Fe LDHs. The contribution to the larger capacitance is partly due to the much larger specific surface area of the micropore defects than that of the outer surface of the electrodes (Table S3). The capacitance of the adsorption and the desorption process implies that the active sites for electrocatalytic OER account for only a small part of the overall surface lattice atoms, and there is still great potential to improve the performance of Co-Fe LDH electrocatalysts *via* more advanced structural design in future work.

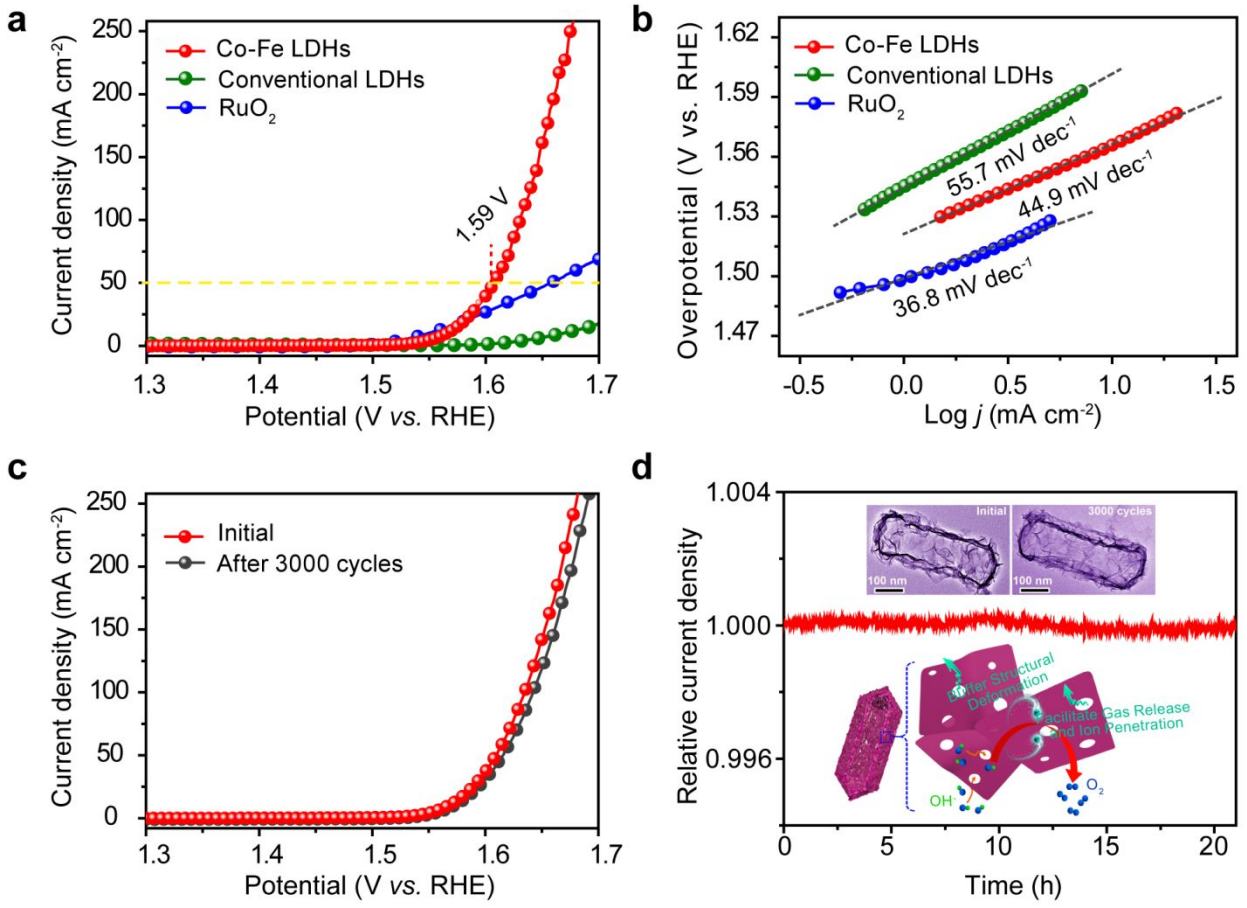

Figure 4. a) Polarization curves and b) Tafel plots in 1 M KOH. c) LSV curves of Co-Fe LDHs before and after 3000 cycles of CV scanning. d) Chronoamperometric measurement at a fixed operating potentials (the inset shows the corresponding TEM images before and after 3000 cycles (upside), and illustration of OER process over Co-Fe LDHs (underside)).

Inspired by the high ionic conductivity and reasonable stability of defect-boosted LDHs in an alkaline environment, we evaluated the appealing OER activity of as-prepared Co-Fe LDHs in a 1 M KOH solution, compared with the conventional LDHs and commercial RuO_2. As illustrated in Figure 4a, Co-Fe LDHs have a low operating potentials of 1.59 V (*vs.* RHE) corresponding to a low overpotential value of 360 mV at a current density (j) of 50 mA cm^{-1}, which is much lower than that of conventional LDHs and commercial RuO_2. As the overpotential increases, the difference of current density of Co-Fe LDHs augments faster than that of RuO_2 and conventional LDHs. To deeply delve into the reaction kinetics of Co-Fe LDHs, we have executed a relevant Tafel analysis, and Figure 4b displays the Tafel slope. The value for Co-Fe LDHs (44.9 mV dec^{-1}) is much lower than that of conventional LDHs (55.7 mV dec^{-1}) and commercial RuO_2 (44.9 mV dec^{-1}). Figure S8 reveals the results of C_{dl}, TOF, and EIS between as-prepared Co-Fe LDHs and conventional LDHs. Compared to the as-prepared Co-Fe LDHs, conventional LDHs manifest lower Tafel slope and TOF values. Besides, their Nyquist plot possesses the larger semicircle diameter in the high frequency region. As expected, the as-prepared Co-Fe LDHs have better performance, which could be caused their hierarchical prismatic structure with a high BET surface area since the conventional LDHs have a lower BET surface area of 20.59 m^2 g^{-1} (Figure S9). To further reveal the intrinsic activities, the LSV curves of different samples were normalized by electrochemical surface area (non-Faradic double layer capacitance), in which the electrochemical surface areas are calculated from double-layer charging curves, assuming a Cdl value of 0.06 mF cm^{-2} for a smooth oxide surface.[40] As seen in Figure S10, the as-prepared Co-Fe LDHs shows the lowest overpotential at a fixed current density, which is basically matched with that in Figure 3a,4a. Altogether, those results demonstrate the prominent catalytic kinetics of Co-Fe LDHs in an alkaline environment. As listed in Table S4, the OER activity of Co-Fe

LDHs in this work is superior or at least comparable to those reported noble-metal-free catalysts of LDHs. Furthermore, the durability and the stability of Co-Fe LDHs for OER in an alkaline environment were investigated. When a sequential CV scanning of 3000 cycles was carried out, the decrease of the current density is negligible compared to the initial density (Figure 4c). Figure 4d exhibits the relative constant current density, referring to the ratio of current density (j) to initial current density (j_0), at a fixed operating potentials, which further demonstrates the promising long-term stability of Co-Fe LDHs. Moreover, as displayed in Figure S11 and the inset (upside) in Figure 4d, the morphology of Co-Fe LDHs remain almost unchanged after the electrochemical aging, and well-defined hierarchical LDH prisms were conserved. After the long-term OER, XRD and XPS characterizations were further executed for the as-prepared Co-Fe LDHs. As seen in Figure S12, the crystal structures of the mentioned sample were inquired, and all the broadened diffraction peaks are nearly indexed to Co-Fe LDHs (JCPDS No. 50-0235). Figure S13 displays the related chemical composition and surface electronic states through XPS analysis. The results of XRD and XPS characterizations towards the as-prepared Co-Fe LDHs after the long-term OER further verify the good stability, as seen in Figure S12,13.

The OER process over the Co-Fe LDHs is depicted in the inset (underside) of Figure 4d. And the structural benefits of LDHs in OER catalysis derived from the intrinsic catalytic activity enhancement can be summarized as the following: (i) the hierarchical prismatic structure of Co-Fe LDHs endows a high BET surface area for ion interaction, thus facilitating the charge transport; (ii) the abundant microporous defects can not only produce wealthy active phase around the pores and notably enrich the active phase, but also provide wettable channels for ion penetration and intimate contact, which is crucial for the remarkably enhanced OER; (iii) the well-distributed microporous defects can serve as an effective buffer area for the volume change,

and then ensure the good electrochemical stability, which refrains from material swelling or severe mechanical deformation during the continuous OER operation.

CONCLUSIONS

In short, defect-boosted Co-Fe LDHs were prepared *via* a facile self-templated strategy and applied as highly efficient OER catalysts. Benefiting from the rich micropore defects with a large number of active sites, the as-prepared Co-Fe LDHs show impressive electrocatalytic performance and stability. It is worth mentioning that the versatility of the microporous structure not only endows the hierarchical LDH prisms with abundant active site exposure, enhanced charge/mass transfer capability, and fast reaction kinetics, but also promises a huge exposed surface and excellent wettability between the electrocatalyst and the electrolyte. The study highlights a cost-effective route to improving the inherent characteristic of noble-metal-free catalysts for gaining deeper insights into electrocatalytic design.

ASSOCIATED CONTENT

Supporting Information

Sectional description of the experimental and corresponding analytical data as well as some additional results

AUTHOR INFORMATION

Corresponding Authors

* C. Ye. E-mail: ye0702@zjut.edu.cn.

* C. H. Ye. E-mail: chye@zjut.edu.cn.

ORCID

Shu-Juan Bao: 0000-0002-2052-2178

Notes

The authors declare no competing financial interest.

ACKNOWLEDGMENTS

C.Y. acknowledges the funding support from the National Natural Science Foundation of China (Grant No. 51771187). C.Y. also thanks the graduate student G.R.H., L.Z.Z. and L.C.Z. at Southwest University.

REFERENCES

(1) Suen, N. T.; Hung, S. F.; Quan, Q.; Zhang, N.; Xu, Y. J.; Chen, H. M. Electrocatalysis for the Oxygen Evolution Reaction: Recent Development and Future Perspectives. *Chem. Soc. Rev.* **2017**, *46*, 337-365.

(2) Wang, M. Q.; Ye, C.; Liu, H.; Xu, M. W.; Bao, S. J. Nanosized Metal Phosphides Embedded in Nitrogen-Doped Porous Carbon Nanofibers for Enhanced Hydrogen Evolution at All pH Values. *Angew. Chem. Int. Ed.* **2018**, *57*, 1963-1967.

(3) Xie, J. F.; Xin, J. P.; Wang, R. X.; Zhang, X. D.; Lei, F. C.; Qu, H. C.; Hao, P.; Cui, G. W.; Tang, B.; Xie, Y. Sub-3 nm Pores in Two-Dimensional Nanomesh Promoting the Generation of Electroactive Phase for Robust Water Oxidation. *Nano Energy* **2018**, *53*, 74-82.

(4) Ye, C.; Wang, Q. M.; Chen, G.; Deng, Y. H.; Li, L. J.; Luo, H. Q.; Li, N. B. One-step CVD Synthesis of Carbon Framework Wrapped Co_2P as a Flexible Electrocatalyst for Efficient Hydrogen Evolution. *J. Mater. Chem. A* **2017**, *5*, 7791-7795.

(5) Stevens, M. B.; Trang, C. D. M.; Enman, L. J.; Deng, J.; Boettcher, S. W. Reactive Fe-Sites in Ni/Fe (Oxy)hydroxide Are Responsible for Exceptional Oxygen Electrocatalysis Activity. *J. Am. Chem. Soc.* **2017**, *139*, 11361-11364.

(6) Rui, K.; Zhao, G. Q.; Chen, Y. P.; Lin, Y.; Zhou, Q.; Chen, J. Y.; Zhu, J. X.; Sun, W. P.; Huang, W.; Dou, S. X. Hybrid 2D Dual-Metal-Organic Frameworks for Enhanced Water Oxidation Catalysis. *Adv. Funct. Mater.* **2018**, *28*, 1801554.

(7) Wang, M. Q.; Tang, C.; Ye, C.; Duan, J. J.; Li, C. M.; Chen, Y. M.; Bao, S. J.; Xu, M. W.; Engineering the Nanostructure of Molybdenum Nitride Nanodot Embedded N-doped Porous Hollow Carbon Nanochains for Rapid All pH Hydrogen Evolution. *J. Mater. Chem. A* **2018**, *6*, 14734-14741.

(8) Guo, M. C.; Zhou, L. X.; Li, Y.; Zheng, Q. J.; Xie, F. Y.; Lin, D. M.. Unique Nanosheet-Nanowire Structured CoMnFe Layered Triple Hydroxide Arrays as Self-Supporting Electrodes for a High-Efficiency Oxygen Evolution Reaction. *J. Mater. Chem. A*, **2019**, *7*, 13130-13141.

(9) Xu, L.; Jiang, Q. Q.; Xiao, Z. H.; Li, X. Y.; Huo, J.; Wang, S. Y.; Dai, L. M.; Wang, S. Y.; Dai, L. M. Plasma-Engraved Co_3O_4 Nanosheets with Oxygen Vacancies and High Surface Area for the Oxygen Evolution Reaction. *Angew. Chem. Int. Ed.* **2016**, *55*, 5277-5281.

(10) Chen, J. D.; Zheng, F.; Zhang, S. J.; Fisher, A.; Zhou, Y.; Wang, Z. Y.; Li, Y. Y.; Xu, B. B.; Li, J. T.; Sun, S. G. Interfacial Interaction between FeOOH and Ni-Fe LDH to Modulate the Local Electronic Structure for Enhanced OER Electrocatalysis. *ACS Catal.*, **2018**, *8*, 11342-11351.

(11) Lu, X. F.; Yu, L.; Lou, X. W. Highly Crystalline Ni-Doped FeP/Carbon Hollow Nanorods as All-pH Efficient and Durable Hydrogen Evolving Electrocatalysts. *Sci. Adv.*, **2019**, *5*, eaav6009.

(12) Sun, P. Z.; Ma, R. Z.; Bai, X. Y.; Wang, K. L.; Zhu, H. W.; Sasaki, T. Single-Layer Nanosheets with Exceptionally High and Anisotropic Hydroxyl Ion Conductivity. *Sci. Adv.* **2017**, *3*, e1602629.

(13) Cai, Z. Y.; Bu, X. M.; Wang, P.; Ho, J. C.; Yang, J. H.; Wang, X. Y. Recent Advances in Layered Double Hydroxide Electrocatalysts for the Oxygen Evolution Reaction, *J. Mater. Chem. A*, **2019**, *7*, 5069-5089.

(14) Zhao, Y. F.; Jia, X. D.; Chen, G. B.; Shang, L.; Waterhouse, G. I. N.; Wu, L. Z.; Tung, C. H.; O'Hare, D.; Zhang, T. R. Ultrafine NiO Nanosheets Stabilized by TiO_2 from Monolayer NiTi-LDH Precursors: An Active Water Oxidation Electrocatalyst. *J. Am. Chem. Soc.* **2016**, *138*, 6517-6524.

(15) Ibrahim, K. B.; Su, W. N.; Tsai, M. C.; Chala, S. A.; Kahsay, A. W.; Yeh, M. H.; Chen, H. M.; Duma, A. D.; Dai, H. J.; Hwang, B. J. Robust and Conductive Magnéli Phase Ti_4O_7 Decorated on 3D-Nanoflower NiRu-LDH as High-Performance Oxygen Reduction Electrocatalyst. *Nano Energy* **2018**, *47*, 309-315.

(16) Jia, Y.; Zhang, L. Z.; Gao, G. P.; Chen, H.; Wang, B.; Zhou, J. Z.; Soo, M. T.; Hong, M.; Yan, X. C.; Qian, G. R.; Zou, J.; Du, A. J.; Yao, X. D. A Heterostructure Coupling of Exfoliated Ni–Fe Hydroxide Nanosheet and Defective Graphene as a Bifunctional Electrocatalyst for Overall Water Splitting. *Adv. Mater.* **2017**, *29*, 1700017.

(17) Wang, Y. Y.; Zhang, Y. Q.; Liu, Z. J.; Xie, C.; Feng, S.; Liu, D. D.; Shao, M. F.; Wang, S. Y. Layered Double Hydroxide Nanosheets with Multiple Vacancies Obtained by Dry Exfoliation as Highly Efficient Oxygen Evolution Electrocatalysts. *Angew. Chem. Int. Ed.* **2017**, *56*, 5867-5871.

(18) Zhou, D. J.; Cai, Z.; Lei, X. D.; Tian, W. L.; Bi, Y. M.; Jia, Y.; Han, N. N.; Gao, T. F.; Zhang, Q.; Kuang, Y.; Pan, J. Q.; Sun, X. M.; Duan, X. NiCoFe-Layered Double Hydroxides/N-Doped Graphene Oxide Array Colloid Composite as an Efficient Bifunctional Catalyst for Oxygen Electrocatalytic Reactions. *Adv. Energy Mater.* **2017**, *8*, 1701905.

(19) Liu, R.; Wang, Y. Y.; Liu, D. D.; Zou, Y. Q.; Wang, S. Y. Water-Plasma-Enabled Exfoliation of Ultrathin Layered Double Hydroxide Nanosheets with Multivacancies for Water Oxidation. *Adv. Mater.* **2017**, *29*, 1701546.

(20) Huang, G.; Xiao, Z. H.; Chen, R.; Wang, S. Y. Defect Engineering of Cobalt-Based Materials for Electrocatalytic Water Splitting. *ACS Sustainable Chem. Eng.* **2018**, *612*, 15954-15969.

(21) Wang, Q.; Shang, L.; Shi, R.; Zhang, X.; Zhao, Y. F.; Waterhouse, G. I. N.; Wu, L. Z.; Tung, C. H.; Zhang, T. R. NiFe Layered Double Hydroxide Nanoparticles on Co, N-

Codoped Carbon Nanoframes as Effcient Bifunctional Catalysts for Rechargeable Zinc–Air Batteries. *Adv. Energy Mater.* **2017**, *7*, 1700467.

(22) Ma, W.; Ma, R. Z.; Wang, C. X.; Liang, J. B.; Liu, X. H.; Zhou, K. C.; Sasaki, T. A Superlattice of Alternately Stacked NiFe Hydroxide Nanosheets and Graphene for Efficient Splitting of Water. *ACS nano* **2015**, *9*, 1977-1984.

(23) Yan, D. F.; Chen, R.; Xiao, Z. H.; Wang, S. Y. Engineering the Electronic Structure of Co_3O_4 by Carbon-Doping for Efficient Overall Water Splitting. *Electrochim. Acta* **2019**, *303*, 316-322.

(24) Yu, Y. F.; Shi, Y. M.; Zhang, B. Synergetic Transformation of Solid Inorganic–Organic Hybrids into Advanced Nanomaterials for Catalytic Water Splitting. *Acc. Chem. Res.* **2018**, *517*, 1711-1721.

(25) Wang, Y. Q.; Yuqin Zou, Y. Q.; Tao, L.; Wang, Y. Y.; Huang, G.; Du, S. Q.; Wang, S. Y. Rational Design of Three-Phase Interfaces for Electrocatalysis. *Nano Research*, **2019**, DOI: 10.1007/s12274-019-2310-2.

(26) Lou, X. W.; Archer, L. A.; Yang, Z. C.; Hollow Micro-/Nanostructures: Synthesis and Applications. *Adv. Mater.* **2008**, *20*, 3987–4019.

(27) Yu, L.; Wu, H. B.; Lou, X. W. Self-Templated Formation of Hollow Structures for Electrochemical Energy Applications. *Acc. Chem. Res.* **2017**, *50*, 293-301.

(28) Yu, L.; Yang, J. F.; Guan, B. Y.; Lu, Y.; Lou, X. W. Hierarchical Hollow Nanoprisms Based on Ultrathin Ni-Fe Layered Double Hydroxide Nanosheets with Enhanced Electrocatalytic Activity towards Oxygen Evolution, *Angew. Chem. Int. Ed.* **2018**, *57*, 172 – 176.

(29) Zhang, J. F.; Liu, J. Y.; Xi, L. F.; Yu, Y. F.; Chen, N.; Sun, S. H.; Wang, W. C.; Lange, K. M.; Zhang, B. Single-Atom Au/NiFe Layered Double Hydroxide Electrocatalyst: Probing the Origin of Activity for Oxygen Evolution Reaction. *J. Am. Chem. Soc.*, **2018**, *140*, 3876-3879.

(30) Burke, M. S.; Kast, M. G.; Trotochaud, L.; Smith, A. M.; Boettcher, S. W. Cobalt-Iron (Oxy)hydroxide Oxygen Evolution Electrocatalysts: The Role of Structure and Composition on Activity, Stability, and Mechanism. *J. Am. Chem. Soc.* **2015**, *137*, 3638−3648.

(31) Nai, J. W.; Lu, Y.; Yu, L.; Wang, X.; Lou, X.W. Formation of Ni–Fe Mixed Diselenide Nanocages as a Superior Oxygen Evolution Electrocatalyst. *Adv. Mater.* **2017**, *29*, 1703870.

(32) Zhang, P.; Lu, X. F.; Nai, J. W.; Zang, S. Q.; Lou, X.W. Construction of Hierarchical Co–Fe Oxyphosphide Microtubes for Electrocatalytic Overall Water Splitting. *Adv. Sci.* **2019**, DOI: 10.1002/advs.201900576.

(33) Fang, Y. J.; Guan, B. Y.; Luan, D. Y.; Lou, X. W. Synthesis of CuS@CoS_2 Double-Shelled Nanoboxes with Enhanced Sodium Storage Properties. *Angew. Chem. Int. Ed.* **2019**, *58*, 7739–7743.

(34) Harrington, S. P.; Devine, T. M. Relation between the Semiconducting Properties of a Passive Film and Reduction Reaction Rates. *J. Electrochem. Soc.* **2009**, *156,* 154-159.

(35) Xu, B.; Fell, C. R.; Chic, M. F.; Meng, Y. S. Identifying Surface Structural Changes in Layered Li-Excess Nickel Manganese Oxides in High Voltage Lithium Ion Batteries: A Joint Experimental and Theoretical Study. *Energy Environ. Sci.*, **2011**, *4*, 2223–2233.

(36) Zhao, J. W.; Chen, J. L.; Xu, S. M.; Shao, M. F.; Zhang, Q.; Wei, F.; Ma, J.; Wei, M.; Evans, D. G.; Duan, X. Hierarchical NiMn Layered Double Hydroxide/Carbon Nanotubes Architecture with Superb Energy Density for Flexible Supercapacitors. *Adv. Funct. Mater.* **2014**, *24*, 2938-2946.

(37) Feng, J. X.; Xu, H.; Dong, Y. T.; Ye, S. H.; Tong, Y. X.; Li, G. R. FeOOH/Co/FeOOH Hybrid Nanotube Arrays as High-Performance Electrocatalysts for the Oxygen Evolution Reaction*Angew. Chem. Int. Ed.* **2016**, *55*, 3694-3698.

(38) Huang, L. L.; Chen, D. W.; Luo, G.; Lu, Y. R.; Chen, C.; Zou, Y. Q.; Y. Q.; Dong, C. L.; Li, Y. F. Wang, S. Y. Zirconium-Regulation-Induced Bifunctionality in 3D Cobalt–Iron Oxide Nanosheets for Overall Water Splitting. *Adv. Mater.* **2019**, 1901439.

(39) Meng, L. X.; Rao, D. W.; Tian, W.; Cao, F. R.; Yan, X. H.; Li, L. Simultaneous Manipulation of O-Doping and Metal Vacancy in Atomically Thin $Zn_{10}In_{16}S_{34}$ Nanosheet Arrays toward Improved Photoelectrochemical Performance, *Angew. Chem. Int. Ed.* **2018**, *57*, 16882-16887.

(40) Bockris, J. O.; Otagawa, T. The Electrocatalysis of Oxygen Evolution on Perovskites. *J. Electrochem. Soc.* **1984**, *131*, 290-302.

TOC Figure

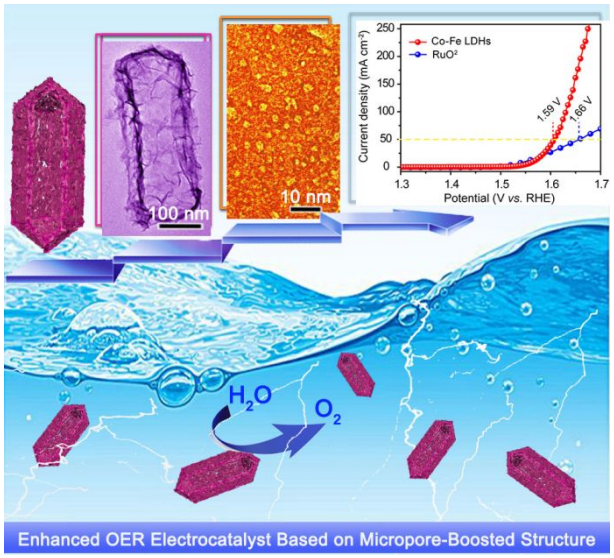
100 nm
10 nm
Co-Fe LDHs
RuO²
Current density (mA cm⁻²)
Potential (V vs. RHE)
1.59 V
1.66 V
H2O
O2
Enhanced OER Electrocatalyst Based on Micropore-Boosted Structure